INTERNATIONAL JOURNAL FOR NUMERICAL METHODS IN FLUIDS
Int. J. Numer. Meth. Fluids 2006; **51**:511–530
Published online 20 December 2005 in Wiley InterScience (www.interscience.wiley.com). DOI: 10.1002/fld.1125

Direct numerical simulation of settling of a large solid particle during bioconvection

P. Geng[‡] and A. V. Kuznetsov[*,†]

Department of Mechanical and Aerospace Engineering, North Carolina State University, Box 7910, Raleigh, NC 27695-7910, U.S.A.

SUMMARY

Settling of a large solid particle in bioconvection flow caused by gyrotactic microorganisms is investigated. The particle is released from the top of the bioconvection chamber; its settling pattern depends on whether it is released in the centre of the bioconvection plume or at its periphery. The Chimera method is utilized; a subgrid is generated around a moving particle. The method suggested by Liu and Wang (*Comput. Fluid* 2004; **33**:223–255) is further developed to account for the presence of a moving boundary in the streamfunction-vorticity formulation using the finite-difference method. A number of cases for different release positions of the particle are computed. It is demonstrated that bioconvection can either accelerate or decelerate settling of the particle depending on the initial position of the particle relative to the plume centre. It is also shown that the particle impacts bioconvection plume by changing its shape and location in the chamber. Copyright © 2005 John Wiley & Sons, Ltd.

KEY WORDS: bioconvection; Chimera method; large particle; motile microorganisms; moving boundary; streamfunction-vorticity formulation; subgrid

1. INTRODUCTION

Bioconvection provides a powerful tool to manipulate mass transfer in microvolumes of fluids. This may have potential pharmaceutical and bio-technological applications. This paper investigates a possible application of bioconvection to control settling of a large solid particle, which may be useful to control sedimentation in microvolumes.

Motile microorganisms swim in a particular direction because of different stimuli such as phototaxis, chemotaxis, or gyrotaxis. This paper considers gyrotactic microorganisms, such

*Correspondence to: A. V. Kuznetsov, Department of Mechanical and Aerospace Engineering, North Carolina State University, Box 7910, Raleigh, NC 27695-7910, U.S.A.
†E-mail: avkuznet@eos.ncsu.edu
‡E-mail: gengpeng@yahoo.com

Contract/grant sponsor: NASA Office of Biological and Physical Research; contract/grant number: NAG3-2706

Received 3 May 2005
Revised 3 May 2005
Accepted 27 September 2005

as many species of algae. Because these microorganisms are bottom heavy, their swimming direction is determined by the balance of gravitational and viscous torques. Gyrotactic behaviour results in the accumulation of these microorganisms in the regions of most rapid downflow. Since the algae are typically 3–5% more dense than water, the density in the regions of downflow becomes larger than in the regions of upflow. Buoyancy increases velocities in both upflow and downflow regions, enhancing velocity fluctuations and introducing a hydrodynamic instability [1–3]. The induced convection fluid motion leads to the development of bioconvection plumes. Many experimental papers [4–7] have described the formation of gyrotactic plumes with regular patterns in algal suspensions.

Geng and Kuznetsov [8, 9] investigated the settling of small solid particles in a suspension of motile gyrotactic microorganisms. It was found that mixing induced by bioconvection slows down settling of such particles which leads to a more uniform number density distribution of solid particles along the height of the chamber. In these studies, the particles were small and their number was large so that they were modelled as a continuous phase having its own number density distribution.

A large number of research papers addressed moving objects in a fluid. Hu *et al.* [10] used the finite element method for the computation of settling a solid object in a liquid. In this study, the motion of the solid object was tracked by an arbitrary Lagrangian–Eulerian (ALE) scheme. Gan *et al.* [11] presented a direct numerical simulation of sedimentation of large solid particles in a flow field induced by natural convection. The cases of one and two large settling particles were investigated. Hsiao and Chahine [12] applied the Chimera method to simulate the bubble dynamics in a vortex flow. A moving Chimera grid was generated to describe the bubble surface motion. Russell and Wang [13] developed a Cartesian grid method for modelling multiple moving objects in a 2-D incompressible viscous flow. An underlying regular Cartesian grid was used to resolve the moving boundary problem. Boundary conditions for the moving boundary were satisfied by superposing a homogeneous solution of Poisson's equation upon the initial solution for the streamfunction. The initial solution was generated by neglecting the moving object in the fluid flow.

The utilization of the streamfunction-vorticity formulation is an effective method for numerical modelling of a 2-D incompressible flow. However, its utilization to calculate the values of the streamfunction and vorticity in a domain that contains moving boundaries still provides a challenge. Liu and Wang [14] introduced a high order finite-difference method in multi-connected domains. This method provides an algorithm for computing boundary conditions for streamfunction and vorticity in a fixed multi-connected domain. In this research, the method developed in Reference [14] is extended to allow for moving boundaries in the domain filled with an incompressible fluid.

This paper considers a large particle (in a 2-D model utilized in this research it is represented by an infinitely long cylinder, see Figure 1(a)) settling in a chamber in which the bioconvection plume is already fully developed. A finite-difference method based on the moving Chimera grid scheme is utilized. The vorticity and streamfunction are introduced into the Navier–Stokes equations to eliminate the pressure.

It is assumed that bioconvection plumes occur periodically. The two-dimensional computational domain coincides either with one or two periodic cells (each periodic cell contains a single bioconvection plume). The height of the periodic cell is H and its width is L, where L is a typical plume spacing and $\lambda = H/L$ is the aspect ratio of the periodic cell. Ghorai and Hill [3] studied the effect of the aspect ratio on bioconvection and found that the steady-state

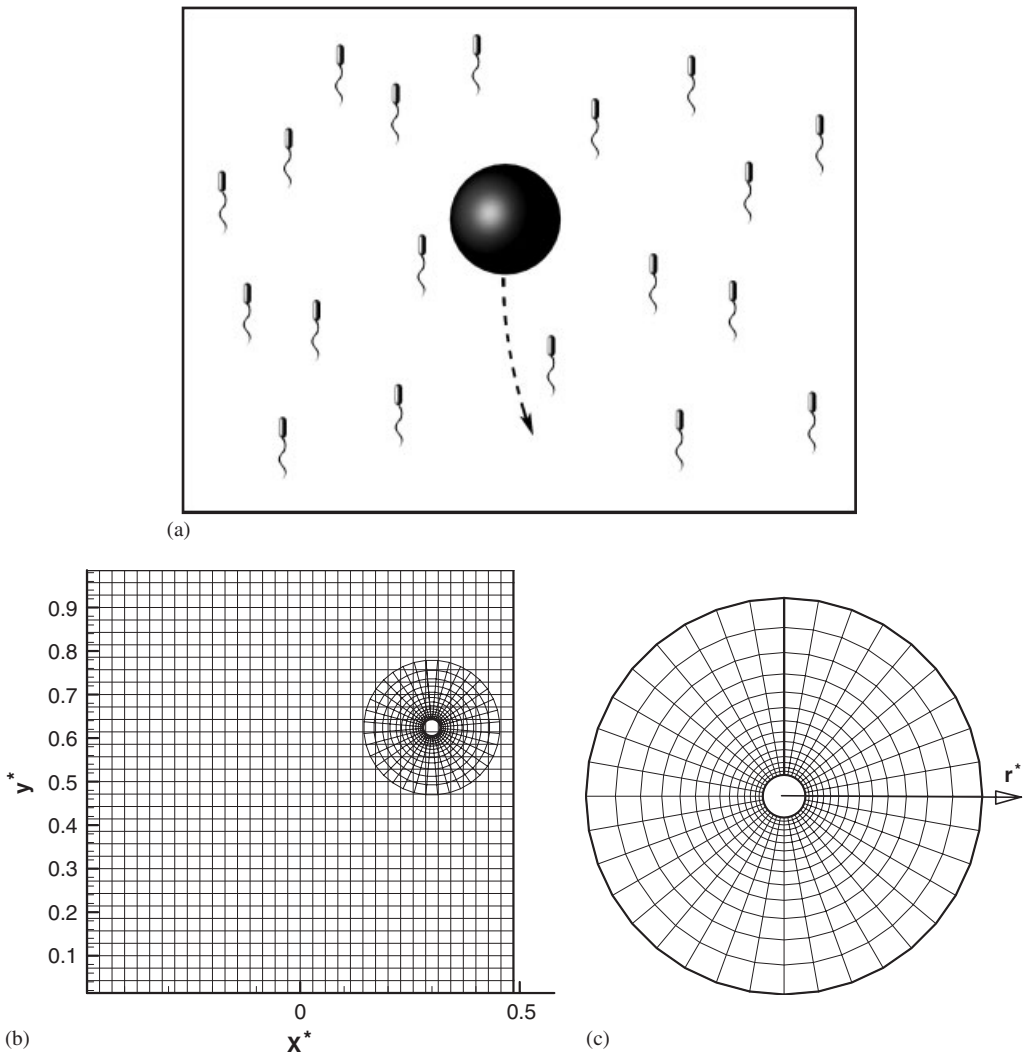

Figure 1. (a) Schematic diagram of a large particle settling in developed bioconvection, flow. Chimera grid system: (b) global and subgrid mesh; and (c) subgrid mesh.

bioconvection plume was stable for $\lambda = 1$. Increasing λ slowed down the solution's convergence to steady-state. This paper assumes that $\lambda = 1$.

2. GOVERNING EQUATIONS

2.1. Dimensional governing equations

Governing equations for a bioconvection plume caused by gyrotactic microorganisms are given in References [2, 3] as

Momentum equation

$$\rho_0 \left(\frac{\partial \mathbf{V}}{\partial t} + (\mathbf{V} \cdot \nabla)\mathbf{V} \right) = -\nabla p_e + \mu \Delta \mathbf{V} + n_m \theta_m \Delta \rho_m \mathbf{g} \tag{1}$$

Continuity equation

$$\nabla \cdot \mathbf{V} = 0 \tag{2}$$

Conservation of motile microorganisms

$$\frac{\partial (n_m)}{\partial t} = -\operatorname{div}(n_m \mathbf{V} + n_m W_m \hat{\mathbf{p}} - D_m \nabla n_m) \tag{3}$$

where D_m is the diffusivity of microorganisms (this assumes that all random motions of microorganisms can be approximated by a diffusive process); n_m is the number density of motile microorganisms; p_e is the excess pressure (above hydrostatic); $\hat{\mathbf{p}}$ is the unit vector indicating the direction of microorganisms' swimming (equations for this vector are obtained in Reference [1]); $\mathbf{V}$ is the velocity vector, (V_x, V_y); $W_m \hat{\mathbf{p}}$ is the vector of microorganisms' average swimming velocity (W_m is assumed to be constant); $\Delta \rho_m$ is the density difference between microorganisms and water, $\rho_m - \rho_0$; θ_m is the volume of a microorganism; μ is the dynamic viscosity of the suspension; and ρ_0 is the density of water.

The motion of the solid particle is described by Newton's second law

$$m \frac{\mathrm{d}V_x}{\mathrm{d}t} = F_x, \quad m \frac{\mathrm{d}V_y}{\mathrm{d}t} = F_y, \quad I \frac{\mathrm{d}\boldsymbol{\omega}}{\mathrm{d}t} = \mathbf{T}$$

and

$$\frac{\mathrm{d}x}{\mathrm{d}t} = V_x, \quad \frac{\mathrm{d}y}{\mathrm{d}t} = V_y, \quad \frac{\mathrm{d}\theta}{\mathrm{d}t} = \omega \tag{4}$$

where $m = \rho_p(\pi d^2/4)$ is the mass of the particle, $I = m(d^2/8)$ is the polar moment of inertia of the particle, d is the diameter of the particle, ω is the particle's angular velocity, $\boldsymbol{\omega}$ is the angular velocity vector, F_x is the x-component of the total external force on the particle, F_y is the y-component of the total external force on the particle, and $\mathbf{T}$ is the mechanical torque on the particle.

The force terms are due to gravity and the viscous force that the fluid exerts on the surface of the particle. Since the particle is symmetric, the viscous friction on the surface of the particle is the only contributor to the torque

$$\begin{aligned} F_x &= \int_\Omega \left(\mu \frac{\partial \mathbf{V}_\tau}{\partial \mathbf{n}} \cdot \hat{\mathbf{x}} \right) \mathrm{d}s \\ F_y &= \int_\Omega \left(\mu \frac{\partial \mathbf{V}_\tau}{\partial \mathbf{n}} \cdot \hat{\mathbf{y}} \right) \mathrm{d}s + \frac{\rho_p - \rho_0}{\rho_p} (\pi d^2/4)\mathbf{g} \\ \mathbf{T} &= \int_\Omega \left(\mu \frac{\partial \mathbf{V}_\tau}{\partial \mathbf{n}} \cdot \frac{d}{2} \right) \mathrm{d}s \end{aligned} \tag{5}$$

where Ω is the surface of the particle and $\mathbf{V}_\tau$ is the tangential fluid velocity along the surface of the particle.

2.2. Dimensionless governing equations

Utilizing the streamfunction-vorticity formulation, the governing equations can be recast in the following dimensionless form:

$$\zeta^* = -\nabla^2 \psi^* \tag{6}$$

$$Sc^{-1}\left(\frac{\partial \zeta^*}{\partial t^*} + V_x^* \frac{\partial \zeta^*}{\partial x^*} + V_y^* \frac{\partial \zeta^*}{\partial y^*}\right) = \nabla^2 \zeta^* - \left(R_\mathrm{m} \frac{\partial n_\mathrm{m}^*}{\partial x^*}\right) \tag{7}$$

$$\frac{\partial n_\mathrm{m}^*}{\partial t^*} = -\nabla \cdot [n_\mathrm{m}^*(\mathbf{V}^* + W_\mathrm{m}^* \hat{\mathbf{p}}) - \nabla n_\mathrm{m}^*] \tag{8}$$

The dimensionless variables in Equations (6)–(8) are defined as

$$\begin{gathered} x^* = \frac{x}{L}, \quad y^* = \frac{y}{L}, \quad t^* = \frac{D_\mathrm{m}}{L^2} t, \quad u^* = \frac{\partial \psi^*}{\partial y^*}, \quad v^* = -\frac{\partial \psi^*}{\partial x^*}, \quad \mathbf{V}^* = \mathbf{V} \frac{L}{D_\mathrm{m}} \\ W_\mathrm{m}^* = W_\mathrm{m} \frac{L}{D_\mathrm{m}}, \quad n_\mathrm{m}^* = \frac{n_\mathrm{m}}{\bar{n}_\mathrm{m}}, \quad Sc = \frac{\nu}{D_\mathrm{m}}, \quad G = \frac{BD_\mathrm{m}}{L^2}, \quad R_\mathrm{m} = \frac{\bar{n}_\mathrm{m} \theta_\mathrm{m} \Delta \rho_\mathrm{m} g L^3}{\rho_0 \nu D_\mathrm{m}} \end{gathered} \tag{9}$$

where asterisks denote dimensionless quantities.

Ghorai and Hill [2, 3] have shown that if the inertia terms in the momentum equation are neglected (which is justified for bioconvection flows because of a very low Reynolds number), the vector $\hat{\mathbf{p}}$, which determines the swimming direction of microorganisms, can be computed as

$$\hat{\mathbf{p}} = \begin{cases} (-\kappa - (\kappa^2 - 1)^{1/2}, 0), & \kappa < -1 \\ (-\kappa, (1 - \kappa^2)^{1/2}), & |\kappa| \leqslant 1 \\ (-\kappa + (\kappa^2 - 1)^{1/2}, 0), & \kappa > 1 \end{cases} \tag{10}$$

where $\kappa = B\zeta = G\zeta^*$. The parameter B is called the 'gyrotactic orientation parameter' by Pedley and Kessler [15], who defined it as

$$B = \frac{4\pi \mu a^3}{mgh} \tag{11}$$

where h is the displacement of the centre of mass of a gyrotactic microorganism from its centre of buoyancy, m is the mass of the microorganism, and a is the radius of a microorganism.

2.3. Chimera grid scheme

The Chimera grid scheme is a grid embedding technique that is utilized in both 2-D and 3-D computations (see, for example Reference [12]). The Chimera scheme provides a simple method for domain decomposition. A structured subgrid is generated around the moving particle settling in bioconvection flow field. In this paper, a subgrid is created around the particle and a global rectangular grid is created for the global flow field, as demonstrated in Figures 1(b) and 1(c). Equations (6)–(8) are solved separately for the global grid and the subgrid. The communication between the global grid and the subgrid is implemented by interpolation. The unknown values of variables in the subgrid boundary points are computed

by interpolating these boundary points onto the global grid with the known values on the global grid. Therefore, the computational problem for the subgrid becomes a boundary value problem. In the global grid, the same procedure is required; the only difference is that an artificial inner boundary is created around the moving particle. The problem for the global grid becomes a boundary value problem by interpolating these artificial inner boundary points onto the subgrid with known values on the subgrid. Equations (6)–(8) are transformed into a polar coordinate system for the subgrid computations.

2.4. Initial and boundary conditions

Equations (6)–(8) are solved subject to the following boundary conditions. The side walls of the computational domain are assumed shear-free in order to model plumes' periodic condition. The free surface is assumed stress-free, and the bottom wall is assumed rigid (a hydrodynamic no-slip condition is imposed there). At the surface of the settling particle, the no-slip boundary condition along with the no-penetration condition for the microorganisms is assumed. Under these assumptions, the boundary conditions at the walls of the computational domain are presented as

$$\psi^* = 0 \text{ at } y^* = 0, \lambda \quad \text{and} \quad x^* = \pm 0.5 \tag{12a}$$

$$\frac{\partial \psi^*}{\partial y^*} = 0 \text{ at } y^* = 0 \tag{12b}$$

$$\frac{\partial^2 \psi^*}{\partial y^{*2}} = 0 \text{ at } y^* = \lambda \quad \text{and} \quad \frac{\partial^2 \psi^*}{\partial x^{*2}} = 0 \text{ at } x^* = \pm 0.5 \tag{12c}$$

Normal fluxes of microorganisms are zero through all boundaries of the computational domain and the surface of the moving particle

$$\mathbf{J}^*_{\mathrm{m}} \cdot \hat{\mathbf{y}} = 0 \text{ at } y^* = 0, \lambda; \quad \mathbf{J}^*_{\mathrm{m}} \cdot \hat{\mathbf{x}} = 0 \text{ at } x^* = \pm 0.5 \tag{13a}$$

$$\mathbf{J}^*_{\mathrm{m}} \cdot \hat{\mathbf{r}} = 0 \text{ at surface of the moving particle} \tag{13b}$$

where $\hat{\mathbf{x}}, \hat{\mathbf{y}}$, and $\hat{\mathbf{r}}$ are the unit vectors in the x-, y- and r-directions, respectively, and

$$\mathbf{J}^*_{\mathrm{m}} = n^*_{\mathrm{m}}(\mathbf{V}^* + W^*_{\mathrm{m}}\hat{\mathbf{p}}) - \nabla n^*_{\mathrm{m}} \tag{14}$$

is the dimensionless flux of microorganisms.

To calculate the values of the streamfunction and vorticity on the moving boundary, they are defined in the polar coordinate system

$$\zeta^* = -\left(\frac{\partial^2 \psi^*}{\partial r^{*2}} + \frac{1}{r^*}\frac{\partial \psi^*}{\partial r^*} + \frac{1}{r^{*2}}\frac{\partial^2 \psi^*}{\partial \theta^2}\right) \tag{15}$$

$$V^*_r = \frac{1}{r^*}\frac{\partial \psi^*}{\partial \theta}, \quad V^*_\theta = -\frac{\partial \psi^*}{\partial r^*} \tag{16}$$

where r^* is the dimensionless radial coordinate, r/L, (see Figure 1(c)) and V^*_r and V^*_θ are the dimensionless velocity components in the polar coordinate system.

Representing $\psi^*(r^*, \theta)$ through Taylor series expansion near the moving boundary and assuming that Δr^* is constant (to simplify equations, the subgrid is constructed such that

the two first grid layers around the particle are of uniform thickness; after that the grid becomes non-uniform) the following equations are obtained:

$$\psi^*(r_0^* + \Delta r^*, \theta) = \psi^*(r_0^*, \theta) + \Delta r^* \frac{\partial \psi^*}{\partial r^*} + \frac{(\Delta r^*)^2}{2} \frac{\partial \psi^{*2}}{\partial^2 r^*} + \frac{(\Delta r^*)^3}{6} \frac{\partial \psi^{*3}}{\partial^3 r^*} + O((\Delta r^*)^4) \tag{17}$$

$$\psi^*(r_0^* + 2\Delta r^*, \theta) = \psi^*(r_0^*, \theta) + 2\Delta r^* \frac{\partial \psi^*}{\partial r^*} + \frac{(2\Delta r^*)^2}{2} \frac{\partial \psi^{*2}}{\partial^2 r^*} + \frac{(2\Delta r^*)^3}{6} \frac{\partial \psi^{*3}}{\partial^3 r^*} + O\big((\Delta r^*)^4\big) \tag{18}$$

where $r_0^* = r_0/L$ and r_0 is the radius of the particle.

Eliminating $(\partial \psi^{*3}/\partial^3 r^*)$ between Equations (17) and (18) and using the expressions for $V_r^*, V_\theta^*, \zeta^*, \partial \psi^*/\partial r^*$, and $\partial^2 \psi^*/\partial r^{*2}$ from Equations (15) and (16), the equation for $\zeta^*(r_0^*, \theta)$ is obtained as

$$\zeta^*(r_0^*, \theta) = \frac{\left(-6\Delta r^* + \frac{2(\Delta r^*)^2}{r_0^*}\right) V_\theta^*(r_0^*, \theta) - (8\psi^*(r_0^* + \Delta r^*, \theta) - \psi^*(r_0^* + 2\Delta r^*, \theta) - 7\psi^*(r_0^*, \theta))}{2(\Delta r^*)^2} - \frac{1}{r_0^*} \frac{\partial V_r^*}{\partial \theta} \tag{19}$$

Liu and Wang [14] have developed a method to calculate the boundary values of the streamfunction on a fixed boundary of a multi-connected domain. In the case of a fixed boundary, the streamfunction is constant along a surface that represents a closed contour in a 2-D space while in the moving boundary case the streamfunction is a function of location (x, y) on the surface and time t. In Reference [14], the momentum equation is multiplied by a unit tangential vector $\boldsymbol{\tau}$ to obtain the boundary condition for the streamfunction. The same idea is utilized in this study for the moving boundary problem.

Multiplying Equation (1) by a unit tangential vector $\boldsymbol{\tau}$ along the moving boundary of the particle, the following is obtained:

$$\rho_0 \left(\frac{\partial \mathbf{V}_\tau}{\partial t} + (\mathbf{V} \cdot \nabla)\mathbf{V}_\tau \right) = -\frac{\partial p_e}{\partial \boldsymbol{\tau}} + \mu \Delta \mathbf{V} \cdot \boldsymbol{\tau} + n_m \theta_m \Delta \rho_m \mathbf{g} \cdot \boldsymbol{\tau} \tag{20}$$

Transforming Equation (20) into the dimensionless form, noting that $\Delta \mathbf{V} \cdot \boldsymbol{\tau} = -(\partial \zeta / \partial \mathbf{n})$, and ignoring the pressure difference along the boundary of the particle (because both bioconvection and settling velocities are small), the following is obtained:

$$\frac{\partial \zeta^*}{\partial \mathbf{n}} = M \tag{21a}$$

$$\text{where} \quad M = -\frac{1}{Sc} \left(\frac{\partial \mathbf{V}_\tau^*}{\partial t^*} + (\mathbf{V}^* \cdot \nabla)\mathbf{V}_\tau^* \right) - R_m n_m \hat{\mathbf{y}} \cdot \hat{\boldsymbol{\tau}} \tag{21b}$$

Discretizing Equation (21a) at the surface of the particle

$$\frac{\partial \zeta^*(r_0^*,\theta)}{\partial \mathrm{n}} = \frac{-3\zeta^*(r_0^*,\theta) + 4\zeta^*(r_0^*+\Delta r^*,\theta) - \zeta^*(r_0^*+2\Delta r^*,\theta)}{2\Delta r^*} = M \tag{22}$$

Substituting Equation (19) into Equation (22) and solving for $\psi^*(r_0^*,\theta)$

$$\begin{aligned}\psi^*(r_0^*,\theta) = &-\frac{4(\Delta r^*)^3 M - 8(\Delta r^*)^2\zeta^*(r_0^*+\Delta r^*,\theta) + 2(\Delta r^*)^2\zeta^*(r_0^*+2\Delta r^*,\theta)}{21} \\ &+\frac{\left(6\Delta r^* - 2\frac{(\Delta r^*)^2}{r_0^*}\right) V_\theta^*(r_0^*,\theta)}{7} + \frac{8}{7}\psi^*(r_0^*+\Delta r^*,\theta) \\ &-\frac{1}{7}\psi^*(r_0^*+2\Delta r^*,\theta) + \frac{2}{7}\frac{(\Delta r^*)^2}{r_0^*}\frac{\partial V_r^*}{\partial \theta}\end{aligned} \tag{23}$$

Equations (19) and (23) provide necessary boundary conditions for the streamfunction and vorticity on the surface of the moving particle.

Initially, at $t^* = 0$, the bioconvection plume is fully developed (see Figure 2). The particle is released with zero initial velocity at some distance beneath the free surface to keep all subgrid nodes inside the computational domain.

2.5. Numerical procedure

A conservative finite-difference scheme is utilized to discretize the governing equations in both Cartesian and polar coordinate systems. An implicit scheme with Euler backward differencing in time and central differencing in space is utilized. A line-by-line tri-diagonal matrix algorithm and iteration technique with over-relaxation for the number density of microorganisms on the global grid and under-relaxation for other variables for both global and subgrid nodal points is used to solve the nonlinear discretized equations. A staggered mesh is utilized in which the streamfunction and vorticity are stored in one nodal set while the number density of microorganisms is stored in another nodal set. The mesh is chosen such that the number density nodes lie in the interior of the computational domain while the streamfunction and vorticity nodes lie in the interior and at the boundary of the domain. Computations are performed on a single 3.0 GHz Intel Xeon processor on the North Carolina State University IBM p690 supercomputer. The typical CPU time required for computing particle settling from just beneath the free surface to near the bottom of the computational domain (on a 36×36 uniform global mesh and a 15×36 non-uniform polar mesh) is approximately 50 h. Numerical stability requires the dimensionless timestep of 2×10^{-7}; the average number of iterations per timestep is 100 (in the beginning of settling the number of iterations is large and it decreases at the settling process goes on). The convergence criterion is that the maximum relative variation of the dimensionless vorticity, streamfunction, and number density of microorganisms in every nodal point between two iterations does not exceed 10^{-7}.

3. RESULTS AND DISCUSSION

Values of the physical properties, geometrical parameters, and dimensionless parameters utilized in computations are summarized in Table I. One of the aims of computations is to

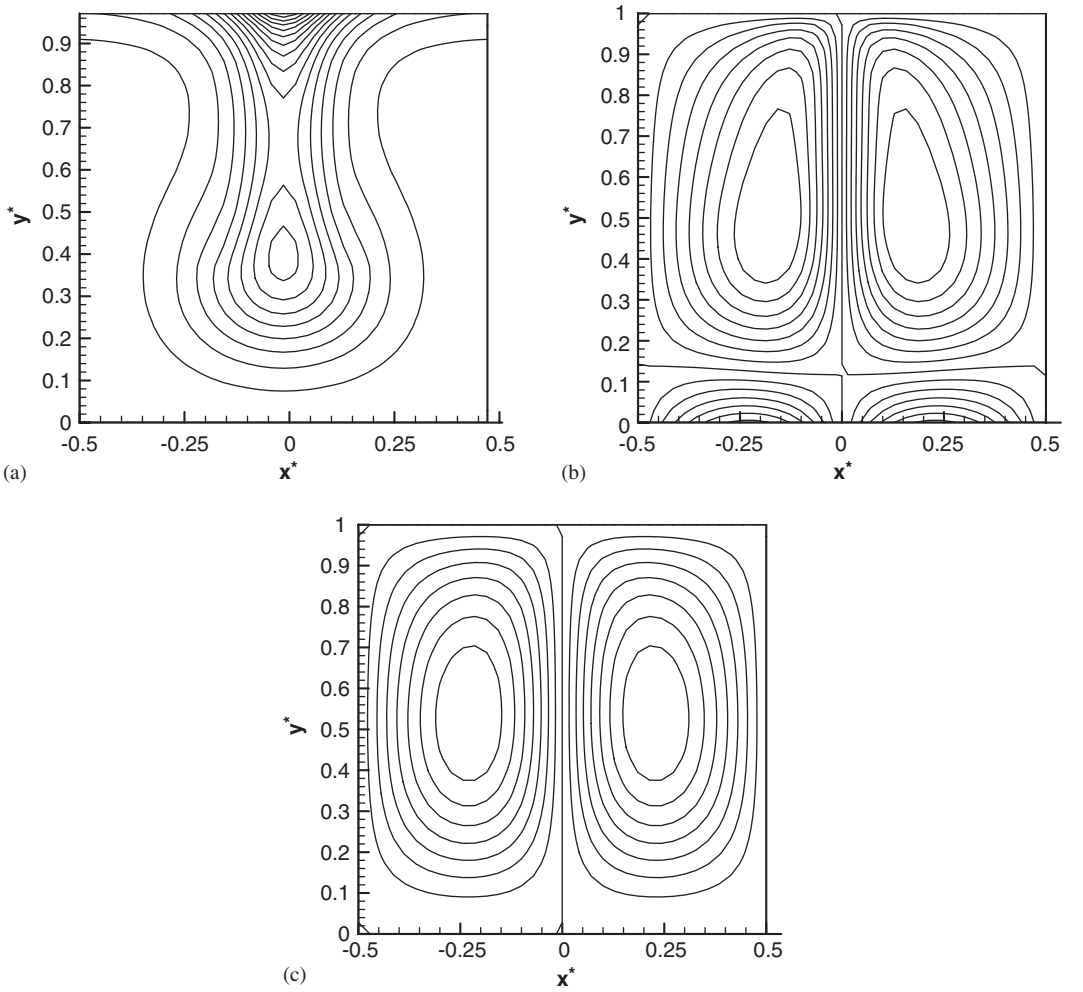

Figure 2. Steady-state bioconvection plume: (a) dimensionless number density of microorganisms; (b) contour lines of the dimensionless vorticity; and (c) contour lines of the dimensionless streamfunction.

investigate the effect of the settling particle on the bioconvection plume. Five cases (A–E) with different particle release positions, different particle densities, and different number of periodic cells (one or two) in the computational domain are investigated. Parameter values for these five cases are summarized in Table II. To ensure that all subgrid point are located within the global mesh, the particle is released at some distance beneath the free surface (the vertical position of the free surface is $y^* = 1.0$, the centre of the particle is initially located at $y^* = 0.8$, the subgrid extends to $r^* = 0.1674$).

Bioconvection is fully developed and steady-state before the particle begins to settle. Figure 2 displays the steady-state bioconvection plume at $t = 0$. Figure 2(a) shows the

Table I. Physical properties, geometrical parameters, and values of dimensionless parameters utilized in computations.

Average number density of microorganisms	$\bar{n}_{\mathrm{m}}$	10^{12} cells/m^3
Density of water	ρ_0	10^3 kg/m^3
Density of microorganisms	ρ_{m}	1.05×10^3 kg/m^3
Volume of a microorganism	θ_{m}	5×10^{-16} m^3
Average swimming velocity of microorganisms	W_{m}	10^{-4} m/s
Diffusivity of microorganisms	D_{m}	5×10^{-8} m^2/s
Gyrotaxis orientation parameter	B	5 s
Kinematic viscosity of the suspension	v	10^{-6} m^2/s
Height of the periodic cell	H	0.005 m
Width of the periodic cell	L	0.005 m
Dimensionless average swimming velocity of microorganisms	$W_{\mathrm{m}}^* = W_{\mathrm{m}} \dfrac{L}{D_{\mathrm{m}}}$	10.000
Schmidt number	$Sc = \dfrac{v}{D_{\mathrm{m}}}$	20
Gyrotaxis number	$G = \dfrac{BD_{\mathrm{m}}}{L^2}$	10^{-2}
Bioconvection Rayleigh number	$R_{\mathrm{m}} = \dfrac{\bar{n}_{\mathrm{m}} \theta_{\mathrm{m}} \Delta\rho_{\mathrm{m}} g L^3}{\rho_0 v D_{\mathrm{m}}}$	612.5
Aspect ratio of the periodic cell	$\lambda = \dfrac{H}{L}$	1
Radius of the particle	r_0	9×10^{-5} m
Density of the particle	ρ_{p}	1.2×10^3 or 1.4×10^3 kg/m^3

Table II. Initial positions of the centre of the particle for Cases A–E.

	Case A	Case B	Case C	Case D	Case E
x^*	0.0	0.3	0.5	0.3	0.3
y^*	0.8	0.8	0.8	0.8	0.8
$\dfrac{\rho_{\mathrm{p}}}{\rho_0}$	1.2	1.2	1.2	1.2	1.4
Number of periodic cells in the computational domain	1	1	2	2	1

dimensionless number density of microorganisms, Figure 2(b) depicts contour lines of the dimensionless vorticity, and Figure 2(c) displays contour lines of the dimensionless stream-function. Number density of microorganisms takes on its maximum value in the centre of the free surface of the computational domain while bioconvection plume is located in the centre of the domain. Fluid flow is directed downward in the centre of the domain and upward at its periphery.

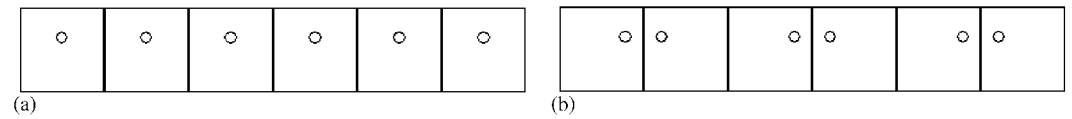

Figure 3. Conditions necessary for periodicity: (a) particle is released in the centre of the chamber; and (b) particle is released at one side of the chamber.

In Case A, the particle is released in the centre of the computational domain, directly in the centre of the falling bioconvection plume. It is assumed that the events happening within the periodic cell are not influenced by other plumes in the neighbouring periodic cells. This assumption implies that neighbouring periodic cells each contain a particle settling in the centre of the cell (see Figure 3(a)). Figure 4 shows the dimensionless number density of microorganisms and contour lines of the dimensionless vorticity and streamfunction at different moments of time ($t^* = 0.0001$ and 0.0007). From Figure 4 it is evident that the settling particle that goes through the bioconvection plume extends the length of the plume. Microorganisms are transported deeper into the chamber by the plume; for example, comparing Figures 4(a) and 2(a) one can see that the local maximum of the number density of microorganisms is displaced downward from $y^* = 0.4$ to approximately $y^* = 0.3$.

Figure 5 shows the dimensionless number density of microorganisms and contour lines of the dimensionless vorticity and streamfunction at different moments of time ($t^* = 0.0001$ and 0.0007) for Case B. As in Case A, it is assumed that the events happening within the periodic cell are not influenced by other plumes in the neighbouring periodic cells. In case B, this assumption implies that the neighbouring periodic cell contains a particle whose initial position is symmetric with respect to the vertical boundary of the periodic cell (see Figure 3(b)). The bioconvection plume is pushed away from the particle during sedimentation. This suggests that the location and the shape of the bioconvection plume can be manipulated by introducing a solid particle into the plume.

To investigate how the upward bioconvection flow affects particle sedimentation, a particle is released between two identical bioconvection plumes (Case C). To compute this case, the width of the computational domain is doubled (in case C it is $2L$) in order to include two periodic cells (see Figure 6). In computing this case, the symmetry of the problem is utilized in the numerical code and the vorticity and streamfunction fields are made antisymmetric with respect to the vertical plane $x^* = 0.5$. Due to this symmetry, the x-viscous force and the torque on the particle vanish.

Figure 6 shows the dimensionless number density of microorganisms and contour lines of the dimensionless vorticity and streamfunction at different moments of time ($t^* = 0.0001$ and 0.0007) for Case C. In the beginning of the process, while the particle settles in the centre of the computational domain, bioconvection plumes, which are located on both sides of the particle, keep their symmetry. As settling continues, the plumes are pushed away from the particle and are shifted to the sides of the domain; their symmetry (with respect to the centreline of the plume) is broken.

To investigate the effect of two neighbouring plumes on particle sedimentation, in Case D (as in case C) a computational domain that consists of two periodic cells is utilized, but, unlike Case C, the particle is released non-symmetrically. The dimensionless distance between the particle release position and the centre of the left bioconvection plume is 0.3 and the distance

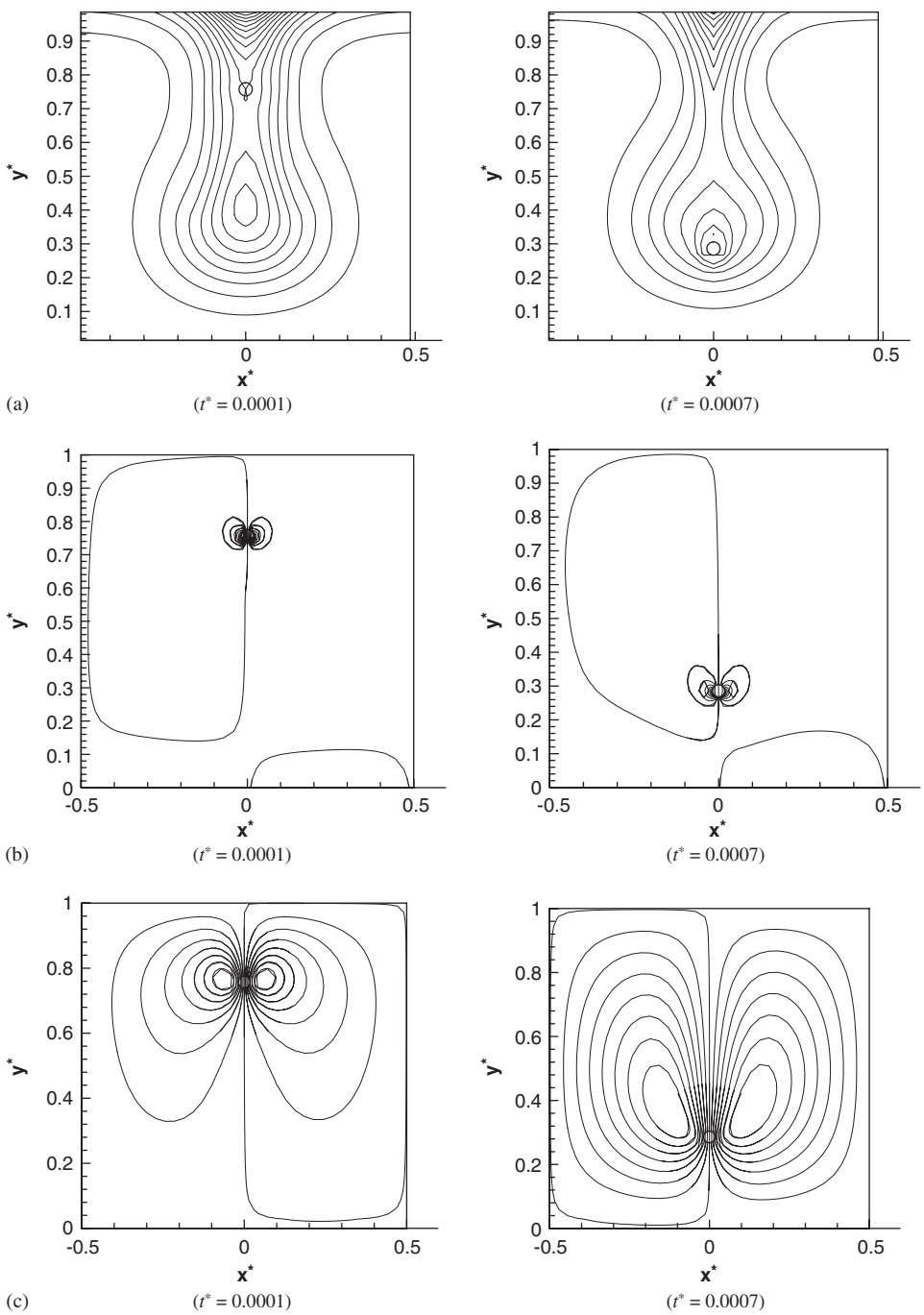

Figure 4. Case A: (a) dimensionless number density of microorganisms; (b) contour lines of dimensionless vorticity; and (c) contour lines of dimensionless streamfunction.

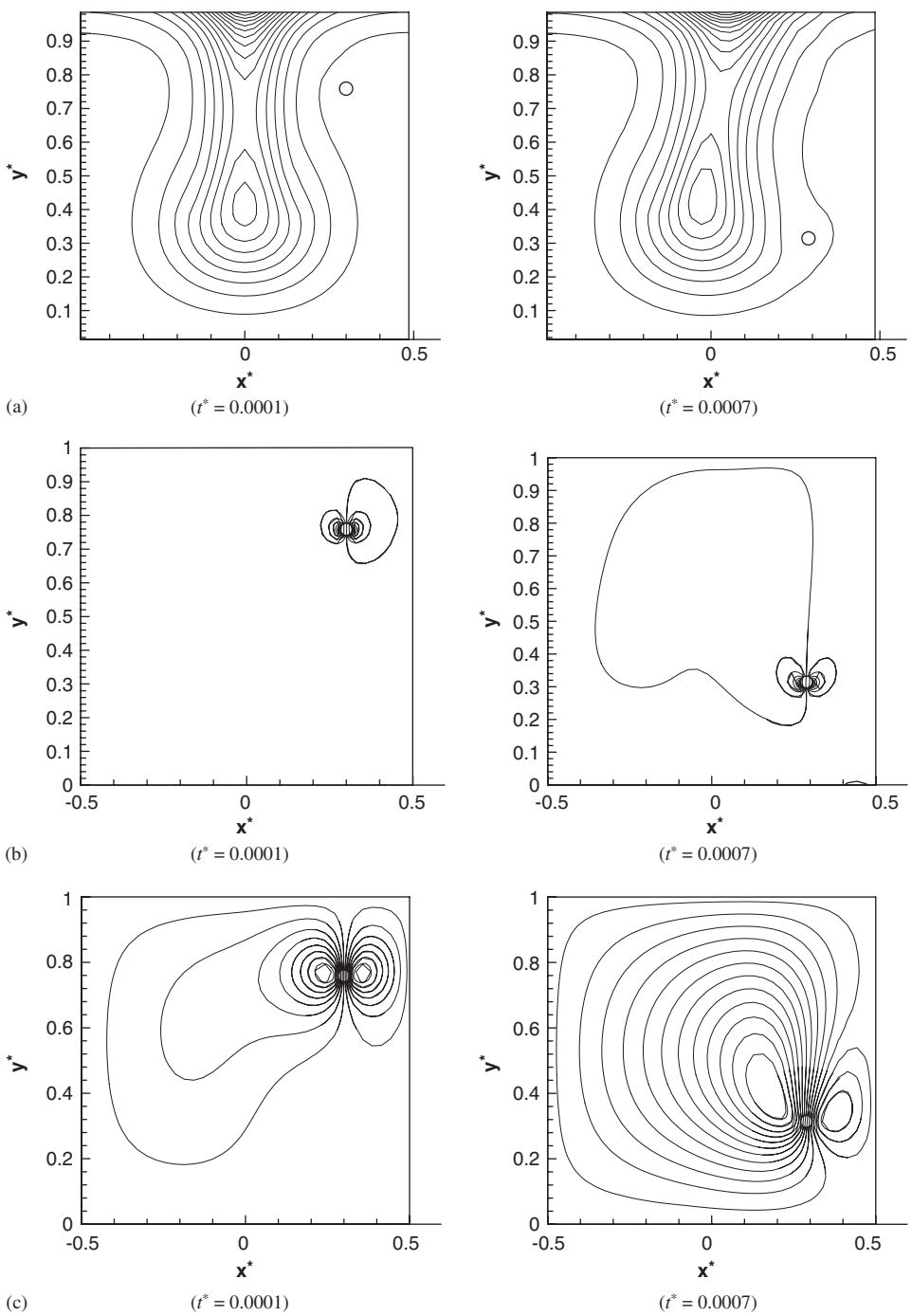

Figure 5. Case B: (a) dimensionless number density of microorganisms; (b) contour lines of dimensionless vorticity; and (c) contour lines of dimensionless streamfunction.

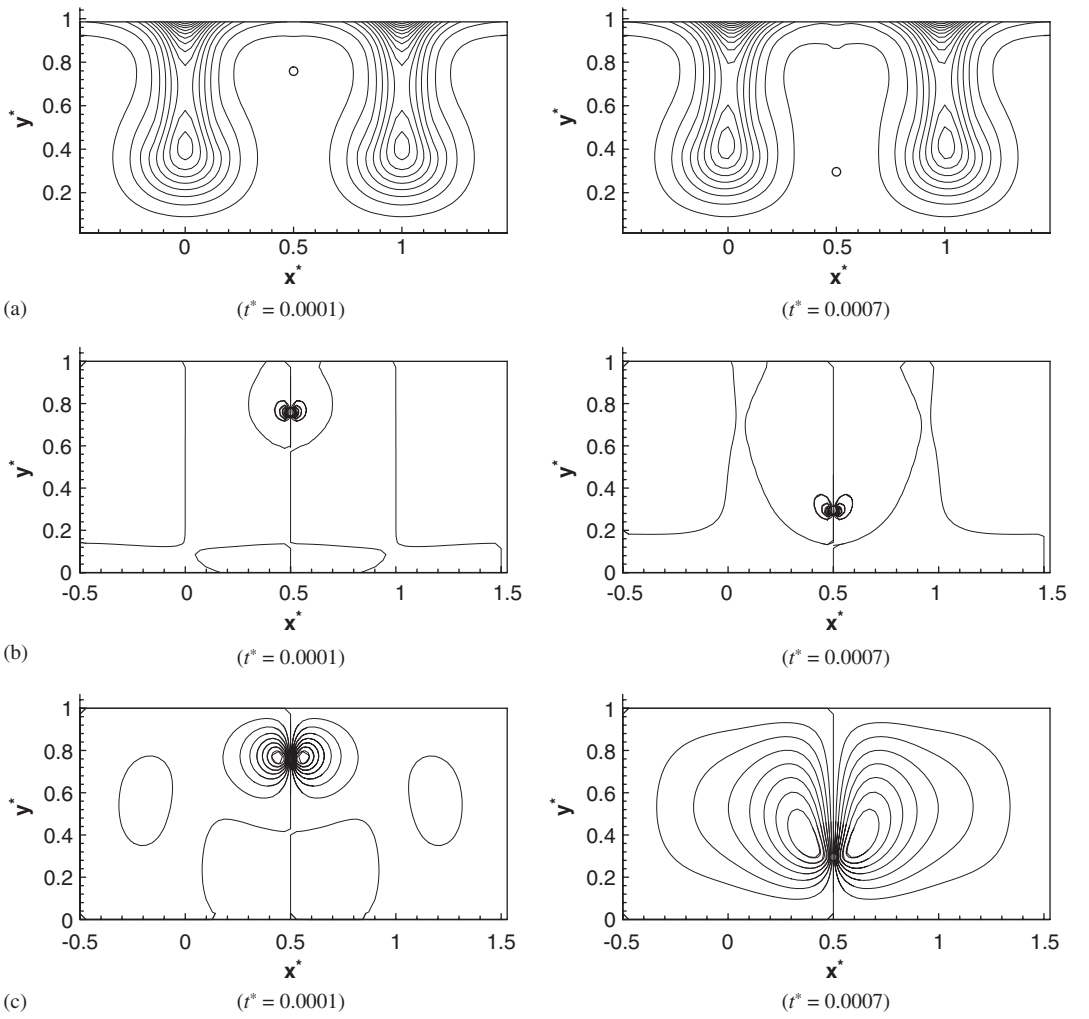

Figure 6. Case C: (a) dimensionless number density of microorganisms; (b) contour lines of dimensionless vorticity; and (c) contour lines of dimensionless streamfunction.

between that and the centre of the right plume is 0.7. Figure 7 shows the dimensionless number density of microorganisms and contour lines of the dimensionless vorticity and streamfunction at different moments of time ($t^* = 0.0001$ and 0.0007) for Case D. The settling particle pushes both bioconvection plumes away as it settles. The left bioconvection plume is pushed farther away than the right one meaning that the particle has more effect on the plume which is closest to it.

Figure 8(a) displays the dimensionless x-velocity of the particle, V_x^*, Figure 8(b) displays the dimensionless y-velocity of the particle, V_y^*, and Figure 8(c) displays the dimensionless angular velocity of the particle, ω^*, for Cases A–C. Figure 8(a) shows that the particle in Case B has the largest x-velocity because the particle is involved in the bioconvection

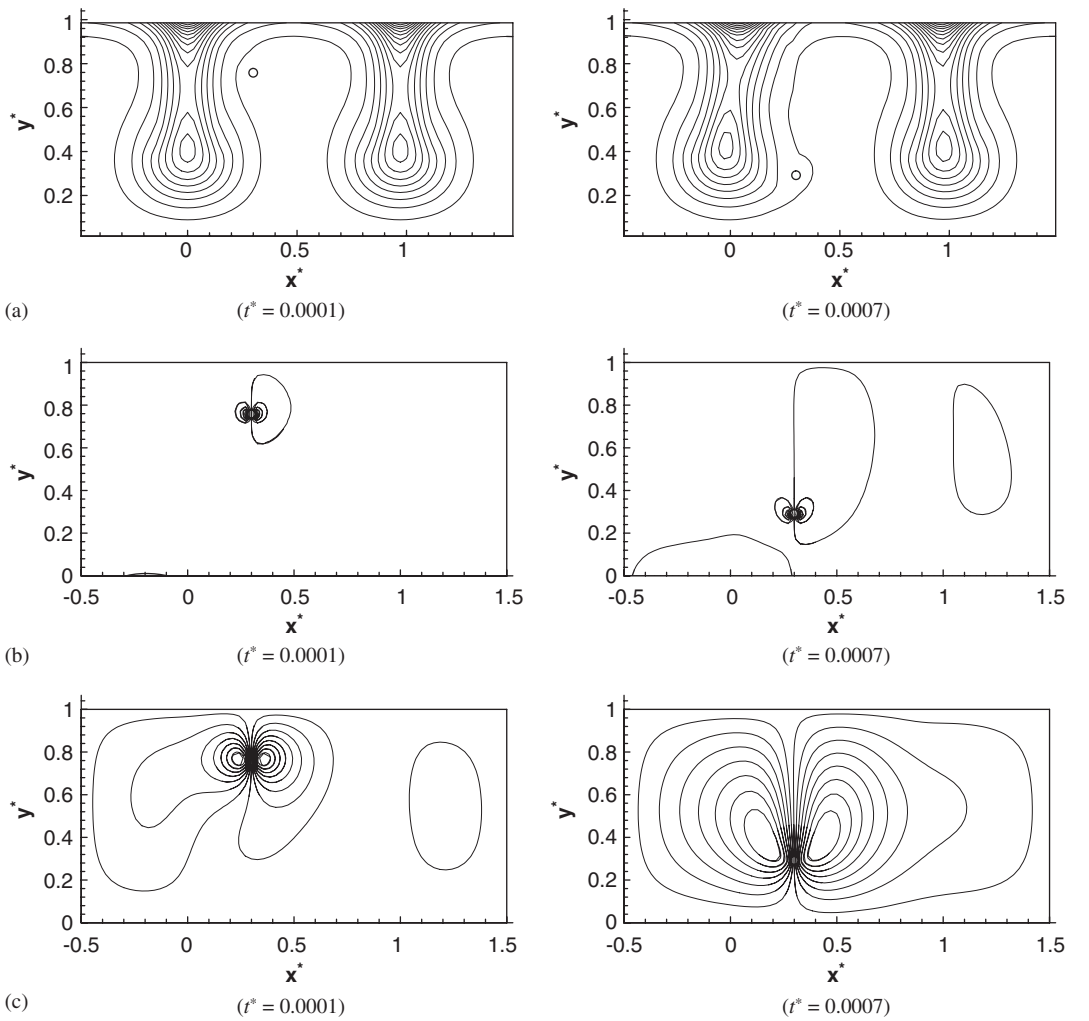

Figure 7. Case D: (a) dimensionless number density of microorganisms; (b) contour lines of dimensionless vorticity; and (c) contour lines of dimensionless streamfunction.

flow, which in Case B at the particle release position has the largest horizontal velocity of the three cases. In Case B the particle is released close to the vertical boundary of the periodic cell. Physically, the largest horizontal displacement of the particle results from the effect of this periodic boundary. In Case D (see Figures 7 and 9) it is shown that if the computational domain is enlarged to include the second periodic cell, the particle displacement in the horizontal direction becomes much smaller. In Cases A and C the bioconvection flow affecting the particle is entirely vertical (the flow is upward for Case C and downward for Case A). Although in Case A the initial position of the particle centre is exactly in the centre of the bioconvection plume, the particle sedimentation is not strictly vertical but shows

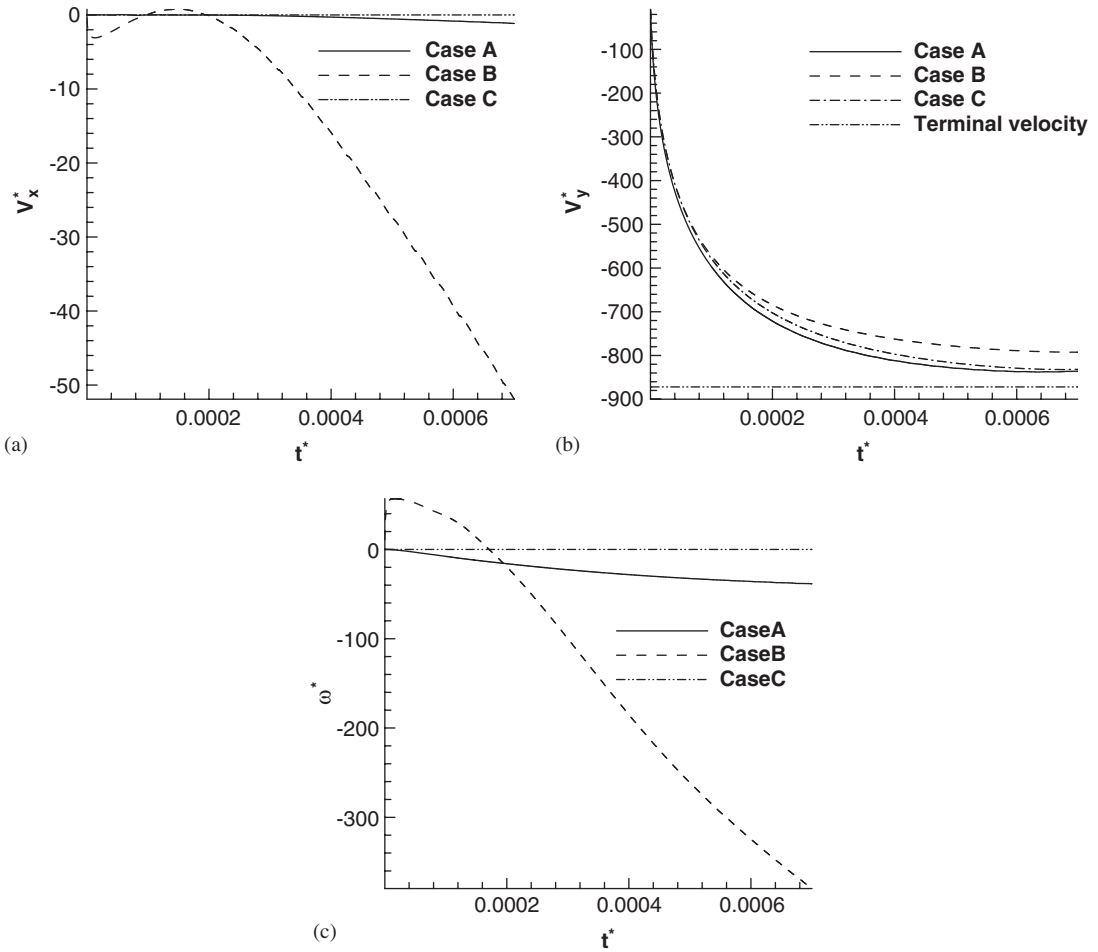

Figure 8. (a) Dimensionless x-velocity, V_x^*, of the particle; (b) dimensionless y-velocity, V_y^*, of the particle; and (c) dimensionless angular velocity of the particle, ω^*, versus time for Cases A, B, and C.

a small (50 times smaller than in Case B) displacement in the horizontal direction. This displacement is caused by numerical inaccuracies. However, there is a different way to look at this result. As particle settles in the centre of the bioconvection plume, a small disturbance (which is modelled by a numerical error in computations) can break the symmetry and make the particle shift to either side. Once the particle is shifted, its displacement from the centre of the domain increases monotonically. This small horizontal velocity is not observed in Case C because, as explained above, the symmetry of the problem is utilized in numerical formulation in computing Case C.

In Figure 8(b), the downward velocity decreases as the particle settles. Its settling y-velocity approaches a constant value, which is the particle terminal velocity caused by the balance of gravitational and viscous forces. The viscous force is calculated using an empirical correlation

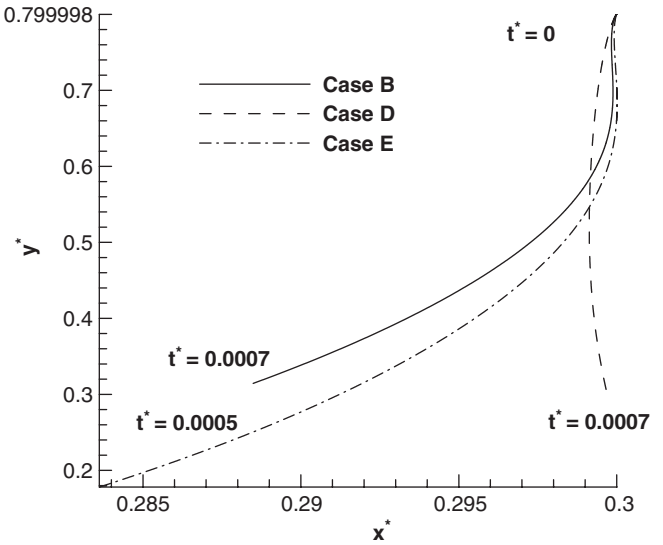

Figure 9. The path of the particle centre for Cases B, D and E.

provided by Sucker and Brauer [16] for a drag coefficient in a flow past a cylinder of unit length

$$C_D = \frac{F_D}{\rho_0 U^2 r_0} \approx 1.18 + \frac{6.8}{Re^{0.89}} + \frac{1.96}{Re^{0.5}} - \frac{0.0004\,Re}{1 + 3.64 \times 10^{-7} Re^2} \tag{24}$$

where $Re = 2Ur_0/v$.

The particle terminal velocity, U, which is shown by a horizontal line in Figure 8(b), is found by equating gravitational and viscous forces

$$F_D = (\rho_p - \rho_0)(\pi r_0^2)g \tag{25}$$

Figure 8(b) shows that particle velocities at the end of the sedimentation process approach the particle terminal velocity (obtained using experimental correlation (24)) in all Cases A–C, which validates the obtained numerical results. This figure also shows that Case A has the largest V_y; this is because the particle release position in this case is in the centre of the plume where the downward velocity of the bioconvection flow is the largest. The absolute value of the downward velocity in Case B is smaller than that in Case C; this happens because the upward bioconvection flow at $x^* = 0.3$ (particle release position for Case B) is stronger than that at $x^* = 0.5$ (particle release position for Case C).

As seen from Figure 8(c), the particle in Case A has a small non-zero angular velocity, which is caused by numerical inaccuracies (physically, because of the symmetry, the particle angular velocity in Case A must be zero). In Case C, the angular velocity of the particle is exactly zero because symmetry of the problem is explicitly utilized in computing this case by making the vorticity and streamfunction fields antisymmetric. In Case B, the angular velocity, ω^*, is decreasing during sedimentation (its absolute value is increasing). This means that the particle rotates in the counter-clockwise direction with an increasing speed.

To study the effect of particle density, a heavier particle is considered in Case E. In this case the particle release position and the computational domain size are identical to Case B. The paths of the particle centres during settling for Cases B, D, and E are displayed in Figure 9. The particle's path for Case E is similar to that for Case B but has larger displacements in both horizontal and vertical directions by the end of sedimentation. In Case D, the particle is displaced toward the centre of the closest plume during the first half of the sedimentation process; this is caused by the direction of the bioconvection flow in the beginning of particle sedimentation. During the second part of the sedimentation process, the direction of the bioconvection flow changes and the particle is displaced away from the centre of the closest plume. The effect of the bioconvection plume in a neighbouring cell is seen from comparing particle's paths for Cases B and D. Neglecting the bioconvection plume in a neighbouring cell and imposing a stress-free impermeable boundary between the two cells results in a larger particle displacement away from this boundary in Case B.

4. CONCLUSIONS

A numerical method based on the streamfunction-vorticity formulation for the case of a multi-connected domain with moving boundaries is developed. This method is utilized to investigate settling of a large solid particle suddenly released in a chamber with a fully developed bioconvection flow caused by gyrotactic microorganisms. The particle settling changes the shape and location of the bioconvection plume. The particle settling is also affected by bioconvection. Because of bioconvection, the particle is pushed in both vertical and horizontal directions. Five different cases are computed with different particle release positions, different particle densities, and different sizes of the computational domain. It is found that restricting the size of the computational domain to one periodic cell by imposing periodic boundary conditions at the vertical boundaries of the domain pushed the particle away from the periodic boundary. Numerical studies involving deeper chambers as well as physical experiments are needed to gain further understanding of this problem.

NOMENCLATURE

a	radius of a microorganism, m
B	time scale for the reorientation of microorganisms by the gravitational torque against viscous torque, $4\pi\mu a^3/mgh$, s
D_{m}	diffusivity of microorganisms, m^2/s
$\mathbf{g}$	gravity vector, $9.81\,\mathrm{m/s}^2$
G	gyrotaxis number, BD_{m}/L^2
h	displacement of the centre of mass of a gyrotactic microorganism from its centre of buoyancy, m
H	height of the chamber, m
$\mathbf{J}^*_{\mathrm{m}}$	dimensionless flux of microorganisms, defined in Equation (14)
L	width of the chamber, m
n_{m}	number density of microorganisms, $1/\mathrm{m}^3$

$\bar{n}_m$	average number density of microorganisms, $1/m^3$
n_m^*	dimensionless number density of microorganisms, $n_m/\bar{n}_m$
$\hat{\mathbf{p}}$	unit vector indicating the direction of swimming of gyrotactic micro-organisms
p_e	excess pressure (above hydrostatic), Pa
r	radial coordinate, m (see Figure 1(c))
r^*	dimensionless radial coordinate, r/L
$\hat{\mathbf{r}}$	unit vector in the r-direction
R_m	bioconvection Rayleigh number, $\bar{n}_m\theta_m\Delta\rho_m g L^3/\rho_0 \nu D_m$
Sc	Schmidt number, ν/D_m
t	time, s
t^*	dimensionless time, $D_m t/L^2$
U	particle terminal velocity, m/s
$\mathbf{V}$	velocity vector, m/s
$\mathbf{V}^*$	dimensionless velocity vector, $\mathbf{V}L/D_m$
V_x	horizontal velocity component, m/s
V_y	vertical velocity component, m/s
V_τ	tangential velocity component, m/s
W_m	average swimming velocity of microorganisms (assumed to be constant), m/s
W_m^*	dimensionless average swimming velocity of microorganisms, $W_m L/D_m$
x	horizontal coordinate, m
x^*	dimensionless horizontal coordinate, x/L
$\hat{\mathbf{x}}$	unit vector in the x-direction
y	vertical coordinate, m
y^*	dimensionless vertical coordinate, y/L
$\hat{\mathbf{y}}$	unit vector in the y-direction

Greek symbols

$\Delta\rho_m$	density difference between microorganisms and water, $\rho_m - \rho_0$, kg/m^3
ζ	horizontal component of vorticity, $1/s$
ζ^*	dimensionless horizontal component of vorticity, $\zeta L^2/D_m$
θ_m	volume of a microorganism, m^3
λ	aspect ratio of the periodic cell, H/L
μ	dynamic viscosity, assumed to be approximately the same as that of water, kg/ms
ν	kinematic viscosity, assumed to be approximately the same as that of water, m^2/s
ρ_0	density of water, kg/m^3
ρ_m	density of microorganisms, kg/m^3
ρ_p	density of the particle, kg/m^3
ψ	streamfunction, m^2/s

ψ^* dimensionless streamfunction, ψ/D_m
ω angular velocity, $1/s$
ω^* dimensionless angular velocity, $(L^2/D_m)\omega$

ACKNOWLEDGEMENTS

AVK gratefully acknowledges Grant #NAG3-2706 awarded to him by NASA Office of Biological and Physical Research, Physical Sciences Division. The authors are indebted to the reviewers whose critical comments helped improving this manuscript.

REFERENCES

1. Pedley TJ, Hill NA, Kessler JO. The growth of bioconvection patterns in a uniform suspension of gyrotactic microorganisms. *Journal of Fluid Mechanics* 1988; **195**:223–338.
2. Ghorai S, Hill NA. Development and stability of gyrotactic plumes in bioconvection. *Journal of Fluid Mechanics* 1999; **400**:1–31.
3. Ghorai S, Hill NA. Periodic arrays of gyrotactic plumes in bioconvection. *Physics of Fluids* 2000; **12**:5–22.
4. Kessler JO. Hydrodynamic focusing of motile algal cells. *Nature* 1985; **313**:218–220.
5. Kessler JO. Co-operative and concentrative phenomena of swimming microorganisms. *Contemporary Physics* 1985; **26**:147–166.
6. Kessler JO, Wiseley DA, Remick KE, Marthaler DE. Individual and collective dynamics of swimming bacteria. In *Proceedings of the Workshop Traffic and Granular Flow'97*, Schreckenberg M, Wolf DE (eds). Springer: New York, 1997; 37–51.
7. Kessler JO, Burnett GD, Remick KE. Mutual dynamics of swimming microorganisms and their fluid habitat. In *Nonlinear Science at the Dawn of the 21st Century*, Christiansen PL, Sorensen MP, Scott AC (eds). Springer: New York, 2000; 409–426.
8. Geng P, Kuznetsov AV. Settling of bidispersed small solid particles in a dilute suspension containing gyrotactic micro-organisms. *International Journal of Engineering Science* 2005; **43**:992–1010.
9. Geng P, Kuznetsov AV. Introducing the concept of effective diffusivity to evaluate the effect of bioconvection on small solid particles. *International Journal of Transport Phenomena* 2005, in press.
10. Hu HH, Joseph DD. Direct simulation of fluid particle motions. *Theoretical and Computational Fluid Dynamics* 1992; **3**:285–306.
11. Gan H, Chang J, Feng J, Hu H. Direct numerical simulation of the sedimentation of solid particles with thermal convection. *Journal of Fluid Mechanics* 2003; **481**:385–411.
12. Hsiao C-T, Chahine GL. Numerical simulation of bubble dynamics in a vortex using Navier–Stokes computations and moving Chimera scheme, 2001; *CAV2001*, *session A10.001*.
13. Russell D, Wang ZJ. A cartesian grid method for modeling multiple moving objects in 2D incompressible viscous flow. *Journal of Computational Physics* 2003; **191**:177–205.
14. Liu J-G, Wang C. High order finite difference methods for unsteady incompressible flows in multi-connected domains. *Computers and Fluids* 2004; **33**:223–255.
15. Pedley TJ, Kessler JO. The orientation of spheroidal micro-organisms swimming in a flow field. *Proceedings of the Royal Society of London*, *Series B* 1987; **231**:47–70.
16. Sucker D, Brauer H. Fluiddynamik bei der angeströmten Zylindern. *Wärme und Stoffübertragung* 1975; **8**:149–158.

